Molecular Recognition and Band Alignment in 3-D Covalent Organic Frameworks for Co-Crystalline Organic Photovoltaics

*Jordan M. Cox‡, Bradley Mileson‡, Ananthan Sadagopan‡, Steven A. Lopez‡**

steven.lopez@northeastern.edu

‡Department of Chemistry and Chemical Biology, Northeastern University, 805 Columbus Avenue, ISEC 355, Boston, MA 02120

Abstract: Covalent organic frameworks (COFs) have emerged as versatile, functional materials comprised of low-cost molecular building blocks. The permanent porosity, long-range order, and high surface area of 3D-COFs permit co-crystallization with other materials driven by supramolecular interactions. We designed a new subphthalocyanine-based 3-D covalent organic framework (**NEUCOF1**) capable of forming co-crystals with fullerene (C_{60}) via periodic ball-and-socket binding motifs. The high co-crystalline surface area and long-range order of **NEUCOF1** eliminates the typical surface area vs. structural order trade-off in organic photovoltaics (OPVs). We used plane-wave density functional theory (PBE) to minimize **NEUCOF1** and **NEUCOF1**–C_{60} co-crystals and determine their electronic band structures. Molecular dynamics (MD) simulations showed that dispersive interactions promoting co-crystallinity **NEUCOF1**–C_{60} are stable up to 350 K. The band structures at 0 and 350 K suggest that there is a driving force of 0.27 eV for exciton charge transfer to the pocket-bound fullerenes. Charge separation could then occur at the COF-C_{60} D-A interface, followed by the transfer of the free electron to the nanowire of C_{60} acceptors with a driving force of 0.20 eV.

Introduction

Highly efficient photovoltaic (PV) technologies which harness the Sun's energy could hold the key to simultaneously eliminating reliance on fossil fuels and preventing further damage to the climate. Unlike inorganic and perovskite solar cells, organic photovoltaics (OPVs) are constructed from low-cost Earth-abundant materials and feature straightforward device fabrication.[1-2] However, current power conversion efficiencies (PCEs) in OPV devices exceed only 14% and 17% for single junction and tandem devices, respectively, and have plateaued in recent years.[3-4] PCEs in current OPV devices are thought to be limited by the active layer architecture due to the competition between structural order and donor-acceptor surface area, where charge separation occurs. The planar heterojunction (PHJ) architecture maximizes structural order but has minimal D-A surface area, limiting the opportunities for charge separation. Bulk heterojunction (BHJ) devices blend the donor and acceptor materials, increasing their interfacial surface area while substantially reducing long-range order. This increases charge recombination via local charge traps

and substantially reduces directional free-charge diffusion pathways.[5] Overcoming this PCE plateau is possible by continuing to develop the nascent co-crystalline OPV architecture that simultaneously maximizes both long-range order and D-A surface area.

One class of materials of particular interest as electron-donating scaffolds in co-crystalline OPVs are covalent organic frameworks (COFs). COFs were first reported by Yaghi and co-workers;[6] they are an exceptional class of permanently porous materials comprised of organic, synthetically accessible building blocks linked together in at least two dimensions. Often arranged in dispersion-bound 2D sheets, COFs exhibit empty channels formed by the aligned pores of adjacent sheets. Many examples of 2D COFs, and some 3D COFs, have been recently applied to separations[7-8], catalysis[9-11], and organic electronics[12-14], including OPVs,[15-16] and have been the subject of rigorous computational study.[17-21] Bein and co-workers reported the first COF OPV device; they demonstrated that charge-separation could be achieved from the electronically excited COF to guest fullerene derivatives.[22] A landmark study by Jiang and co-workers reported the highest PCE for a COF-based OPV measured to date, 0.9%.[23] Despite the improvements made by Jiang and co-workers, PCEs in COF OPVs are still low. This is due in part to a combination of limited electronic communication between adjacent dispersion-bound COF sheets and poor molecular recognition between the planar COF sheets and curved fullerene acceptors. While COF co-crystals have emerged as a new OPV architecture, next-generation co-crystals will feature 3D-COFs to enhance structural order and molecular recognition of acceptor molecules.

A design strategy that could simultaneously improve both of these factors in COF OPVs is the incorporation of non-planar π-conjugated molecular building blocks.[24] Non-planar π-conjugated molecules are known to recognize fullerenes in solution and various co-crystals have been published.[25-27] Their complementary shapes promote dispersion complexation through extended π-orbital overlap. Additionally, non-planar systems facilitate the formation of 3-D periodic COF materials, increasing the electronic coupling between adjacent COF sheets through covalent bonds. Inspired by this concept, we have designed a light-responsive, synthetically-accessible 3-D COF, **NEUCOF1**, based on non-planar π-conjugated boron-subphthalocyanine (SubPcs, Figure 1) building blocks. These have well-documented syntheses and functionalization at peripheral and axial sites. Their absorption maximum ranges from 550-600 nm, making them ideal candidates to absorb sunlight.[28] SubPcs have been incorporated into several BHJ OPV devices[29-31] because of

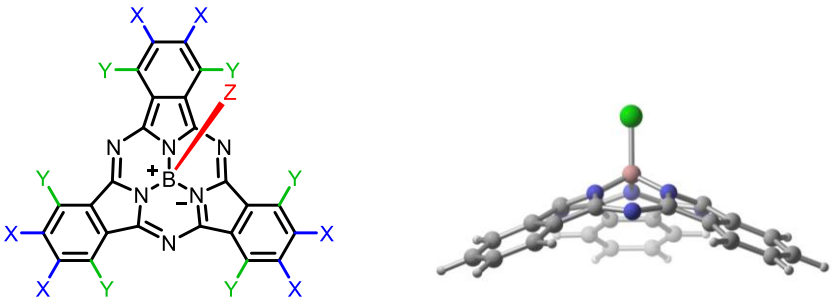

Figure 1. (Left) Chemical structure of a SubPc molecule with highlighted peripheral (blue X, green Y) and axial (red Z) positions. (Right) DFT-optimized geometry.

their ability to form dispersion complexes with C_{60} molecules in a ball-and-socket motif, in 1:1 and 2:1 ratios.[25, 32-33] These complexes are also well known to undergo charge-transfer upon light absorption by SubPc to the dispersion-bound C_{60}, further supporting our choice to pursue SubPc-

based co-crystalline COFs.[34-35] **NEUCOF1** is a 3-D COF material entirely comprised of periodically linked functionalized SubPc molecules. Ong and Swager recently demonstrate the self-correcting synthesis of thianthrene-based COFs via the condensation of 1,2-dithiols and 1,2-difluoro compounds.[36] This chemistry could possibly be extended to **NEUCOF1** because of the intended thianthrene-like connection.

Computational Methods

PW-DFT calculations were performed using the projector-augmented wave (PAW) method with the PBE exchange-correlation functional as implemented in the Vienna Ab initio Simulation Package (VASP).[37-40] A kinetic energy cutoff of 400 eV was used with a 2x2x2 Monkhorst-Pack k-point grid and Grimme's D3 empirical dispersion correction with Becke-Johnson damping.[41] Initial models of **NEUCOF1** and COF-C_{60} co-crystals were relaxed using a variable cell algorithm until forces were less than 0.02 eV $Å^{-1}$ per atom, and band structures, densities-of-states (DOS), and Γ-point partial charge densities were computed for these relaxed structures. DFT methods qualitatively reproduce band structures in semiconductor materials with the exception that the absolute value of the band gap is categorically underestimated, known as the band gap problem.[42] Therefore, the computed PBE band structures discussed herein are interpreted qualitatively, without relying on the value of the band gap energy. The band structures for all models were calculated along the high-symmetry path for hexagonal cells determined by Setyawan and Curtarolo (see SI).[43] Partial charge densities and the band structure high-symmetry path were visualized using the VESTA 3D visualization package.[44] DOSs were computed on a more dense 6x6x6 k-point grid.

We estimated the band gap energy of **NEUCOF1** by computing the energy gap between the highest occupied molecular orbital (HOMO) and the lowest unoccupied molecular orbital (LUMO) for oligomeric fragments of the COF. To this end, we used the hybrid density functional B3LYP[45] with the aug-cc-PVDZ[46-48] basis set. The HOMO-LUMO gap for a single SubPc monomer as well as a dimer, trimer, and tetramer were computed and plotted as a function of $1/N$, where N is the number of monomer units. This data was fit to a linear function and extrapolated to infinite monomers.

Molecular dynamics simulations were performed with the LAMMPS molecular dynamics program[49] using the OPLS3 all-atom force field.[50] Models were initially relaxed at 10 K, then heated over 100 ps to 350 K. After heating, the simulations were propagated for 2 ns and the stability of these simulations was determined by RMSD analysis, shown in the Supporting Information. All final structures are based on the 2 ns production runs with the canonical (NVT) ensemble. Simulations were performed on three different co-crystalline models. Two of these models utilize a truncated **NEUCOF1** model which includes a single unidirectional channel and maximizes the available surface area in the other two directions, resulting in a 1D wire analogue of **NEUCOF1**, see the Supporting Information. The 1D wire analogue allows our simulations to probe the interactions of the COF with acceptor molecules near the surface. The other simulation uses a fully 3-D periodic model equivalent to the model of co-crystal **C**, described below. Full simulation details are provided in the Supporting Information.

Results and Discussion

We have employed plane-wave density functional theory (PW-DFT) calculations to minimize the periodic structure of **NEUCOF1** (Figure 2). **NEUCOF1** exhibits regular 17.4 Å binding pockets, suitable for fullerene or other acceptor molecules, which are formed between adjacent COF sheets. The sheets are linked by alkynyl connectors and are typically spaced by 4.3 Å (B–B

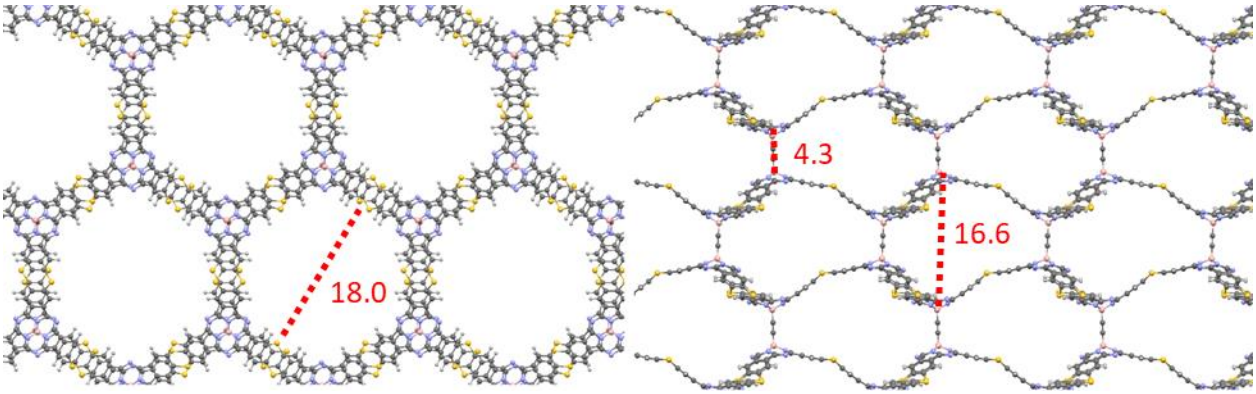

Figure 2. PW-DFT relaxed geometry of **NEUCOF1**. Views (left) along and (right) orthogonal to the hexagonal channels are shown and correspond to crystallographic directions [001] and [010] in the approximately hexagonal lattice. Widths of hexagonal pores, binding pockets, and sheet spacing are shown in red. Distances are reported in Ångstroms.

distance) in the optimized structures. The COF also exhibits 17.9 Å unidirectional channels formed by the alignment of the hexagonal pores in each sheet. These two types of binding sites, pockets and pores, are well suited to accommodate C_{60} molecules which have a van der Waals diameter of approximately 10 Å. To probe the interactions of **NEUCOF1** with fullerene C_{60} guests, we have also minimized the geometries of three COF-C_{60} co-crystals, **A**, **B**, and **C**. Figure 3 shows the PW-DFT relaxed unit cells of these co-crystals and illustrates the arrangement of fullerenes in each co-crystal.

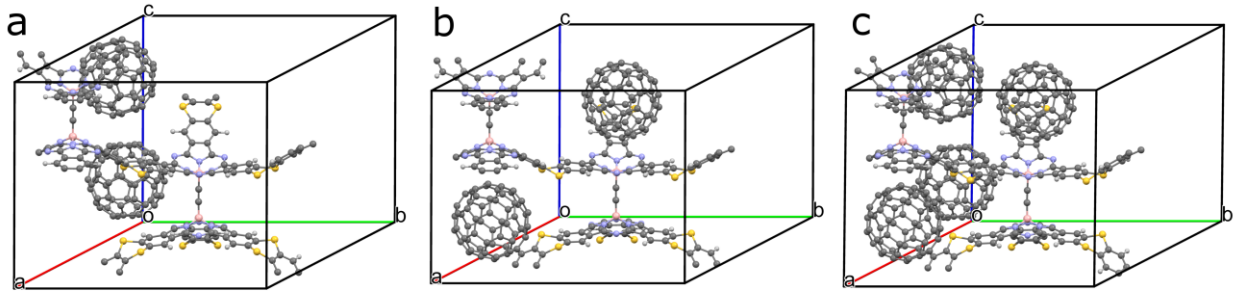

Figure 3. PW-DFT relaxed unit cells for co-crystals (a) **A**, (b) **B**, and (c) **C**.

Co-crystal **A** contains fullerene molecules in the hexagonal channels, **B** contains fullerenes in the binding pockets, and **C** has fullerenes in both binding sites. Figure 4 shows the periodic structures of **A**, **B**, and **C** viewed down the hexagonal channel of the COF to illustrate the locations of the acceptor molecules in the fully periodic models. Figure 4 also shows an orthogonal view of **B** to demonstrate the arrangement of fullerenes in the binding pockets. The interatomic spacing between C_{60} molecules in **C** is important to note here. The two unique pocket-bound fullerene molecules in **C** and their respective nearest neighbor fullerene in the COF channel are 3.1 and 3.0 Å apart. The two unique fullerene molecules in the channel are separated by 2.8 Å.

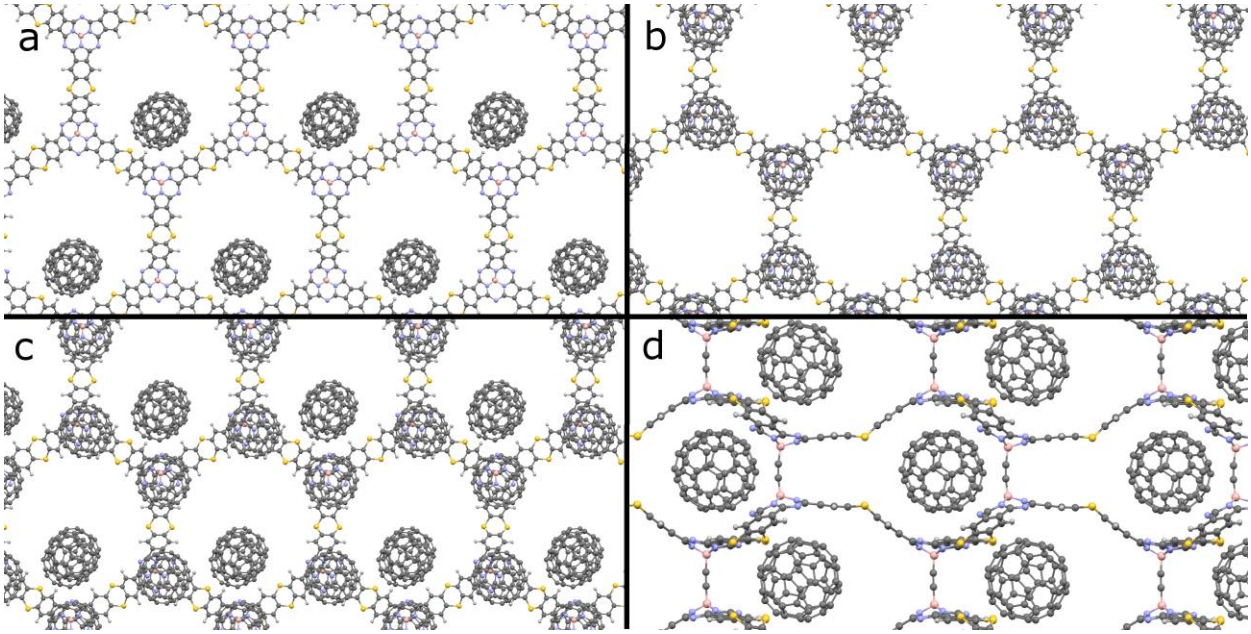

Figure 4. PW-DFT minimized geometries of **A**, **B**, and **C**. (a) View down the hexagonal channel of **A**, along crystallographic direction [001]. (b) View along [001] of **B**. (c) View along [001] of **C**. (d) View orthogonal to [001] of **B**, showing fullerene molecules held in the binding pockets, along crystallographic direction [010].

Electronic structure

To determine the suitability of **NEUCOF1** for photovoltaic applications, we computed the band structures of the COF, and co-crystals **A**, **B**, and **C**. The band structures and corresponding DOS are shown in Figure 5. According to its band structure, **NEUCOF1** is an organic semiconductor with an indirect PBE band gap of 1.36 eV, though it is well known that PBE underestimates this value. A hybrid DFT functional could improve our calculation of the band gap energy, but the computational cost of hybrid DFT methods can be as much as three orders of magnitude greater in the case of PW-DFT. With a 9,700 $Å^3$ unit cell and the 164-404 atoms in the cell, the cost of a hybrid-PW-DFT calculation is prohibitive. Botti and co-workers[51] determined that the PBE functional underestimates band gaps by a median value of 0.8 eV. We estimate the true gap energy to be 2.2 eV for **NEUCOF1** by applying the 0.8 eV correction. We also estimated the true gap energy by computing the HOMO-LUMO gap energy with hybrid-DFT for four **NEUCOF1** clusters featurign one to four SubPc units; a linear fit of these energies estimates a COF band gap energy of 2.25 eV (Figure S4). PBE predicts that the valence band has a width of 0.37 eV and the conduction band that has a width of 0.28 eV. This decreased band width suggests that electrons in the COF conduction band should be more localized than in the valence band.

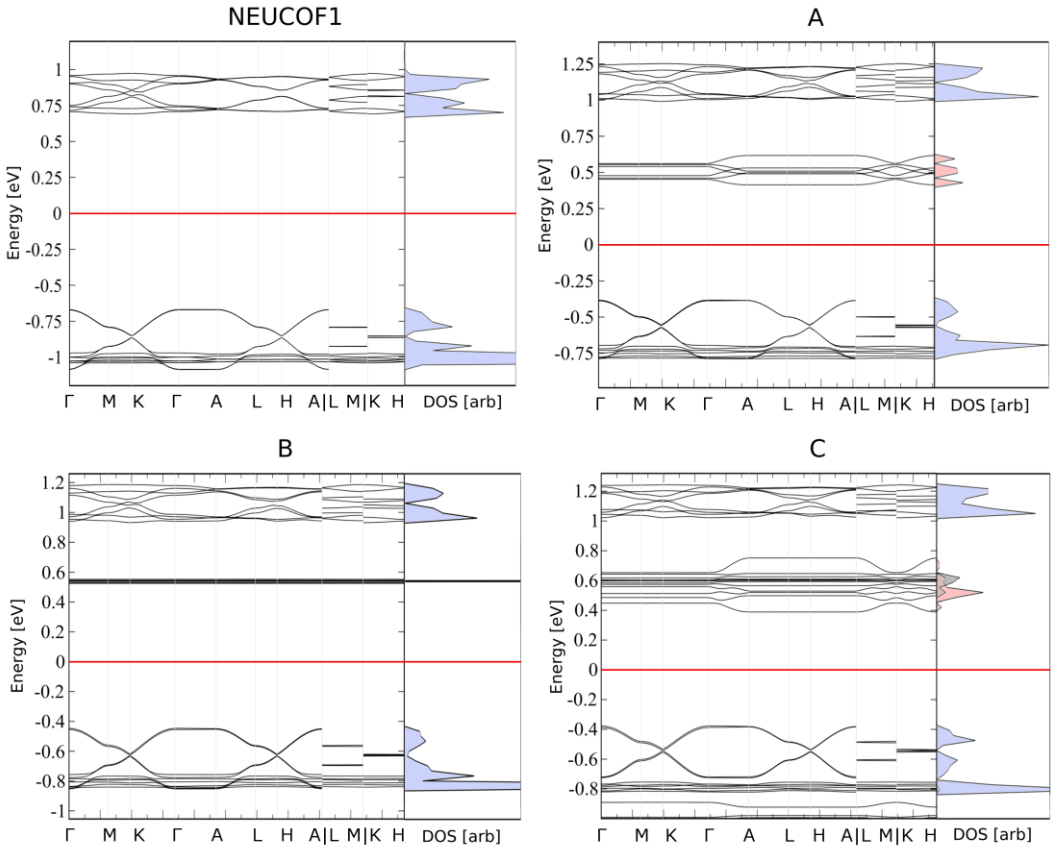

Figure 5. Band structures and densities-of-states plots for (top-left) **NEUCOF1** and co-crystals (top-right) **A**, (bottom-left) **B**, and (bottom-right) **C**. All energies are plotted relative to the Fermi level, shown by the red line, and vertical dashed lines show high-symmetry points. The DOS plots are separated into contributions from the COF (blue), fullerenes in binding pockets (grey), and fullerenes in channels (red).

The band structure of **A** illustrates the new energy bands resulting from the inclusion of fullerenes into the COF channel. The fullerene conduction band (red DOS curve) is composed of six electronic bands which arise from the mixing of the three degenerate LUMOs on each of the two fullerene molecules in the unit cell, and lies within the band gap of the COF. The maximum of the fullerene conduction band lies 0.37 eV below the COF conduction band minimum. This band has a width of 0.20 eV; the conduction band width in crystalline C_{60} is approximately 0.5 eV. The fullerene molecules in **A** should be isoenergetic, so the separation and spreading of their bands indicates that these fullerene molecules are interacting with one another in the co-crystal. This column of interacting fullerenes could form a 1-D nanowire in **NEUCOF1** co-crystals and related co-crystals.

The band structure and DOS of **B** shows the fullerene-localized conduction band in the band gap region of **NEUCOF1**, similar to **A**, 0.38 eV below the COF conduction band minimum. However, the six degenerate bands here are very flat, with a width of 0.03 eV. The fullerene molecules in **B** are housed within the binding pockets of **NEUCOF1**, simultaneously quarantining each fullerene and preserving the degeneracy.

Co-crystal **C** combines the fullerene arrangements of **A** and **B**, and its band structure reflects this with contributions from twelve empty C_{60} orbitals in the conduction band group. The conduction band width for fullerenes in **C** is 0.36 eV, and the conduction band maximum in this

group lies 0.27 eV below the COF conduction band, within the COF band gap. The width of 0.36 eV indicates the presence of significantly delocalized orbitals involving all C_{60} molecules in the cell. The DOS shows that the bands at the top of this group are comprised of states more heavily localized on the pocket fullerenes (grey curve), while the lower-energy bands are more localized on the channel fullerenes (red curve).

These band structures and DOS plots show that the electronic structure of **NEUCOF1** is largely unchanged upon inclusion of fullerene acceptors into the framework. The conduction bands of the fullerenes are aligned well with the band gap of the COF and provide an energetic driving force for **NEUCOF1** → C_{60} charge transfer. The widths of the C_{60} conduction bands in **A** and **C** (0.20, 0.27 eV) indicate a significant degree of orbital overlap between adjacent C_{60} molecules in the COF pores. The relatively close contacts of fullerenes (≤ 3.2 Å) and the delocalized bands suggest that charge-hopping between C_{60} molecules is a possible mechanism of charge transport in the COF.

Γ-point partial charge densities

To develop a chemically intuitive understanding of the electronic structure of **NEUCOF1** and its C_{60} co-crystals, we have computed band-specific partial charge densities at the Γ-point for the most relevant frontier energy bands in **NEUCOF1**, **A**, **B**, and **C**. Figure 6 shows the densities for **C**; the corresponding densities for **NEUCOF1**, **A**, and **B** are nearly identical and are shown in Table S1 of the Supporting Information. The Γ-point densities show that the top valence band is made up of the delocalized π-system of one of the COF sheets. This band is degenerate with another valence band (not shown) which is comprised of the π-system of the other COF sheet in the unit cell. The COF conduction band shows a depletion of electron density, relative to the valence band, at the periphery of the SubPc units *(i.e.*, near the sulfur atoms) with a localization of

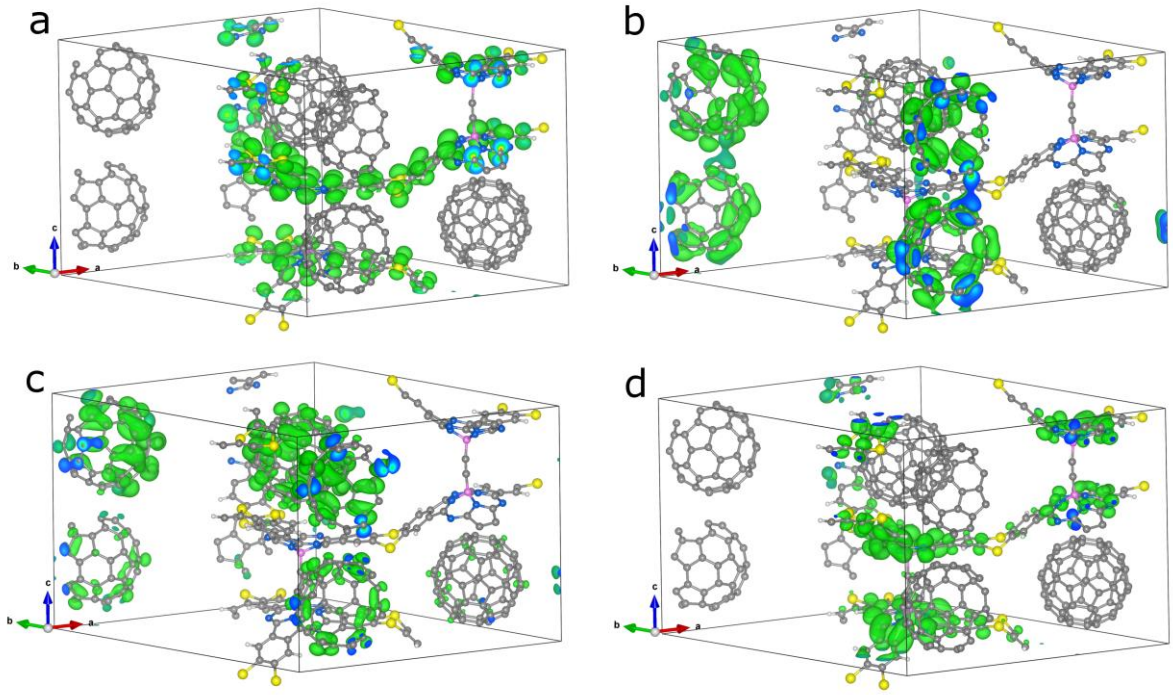

Figure 6. Γ-point partial charge densities for frontier bands in **C**. (Bottom-left) Valence band, (bottom-right) fullerene conduction band minimum, (top-right) fullerene conduction band maximum, and (top-left) the COF conduction band minimum.

this density around the cores of the SubPcs (*i.e.*, near the nitrogen atoms). This localization of density was seen in the band structures in the reduced band width of the COF conduction band relative to the valence band.

The Γ-point density for the fullerene conduction band maximum shows shared density between one pocket-bound fullerene and one channel fullerene. This delocalized electron density indicates the presence of significant intermolecular orbital overlap. The density localized on the pocket-bound fullerene in this partial charge density overlaps significantly with the density of the COF conduction band. This high degree of overlap promotes charge transfer from the COF to C_{60} molecules in the binding pockets, just as it does in SubPc-C_{60} molecular complexes.[25, 34-35] Thus excitation of the COF should generate a COF-localized exciton which will experience a 0.27 eV driving force for charge transfer to a fullerene acceptor in a nearby binding pocket.

The C_{60} conduction band minimum density shows shared electron density between the two fullerene molecules in the channel, forming a 1-D fullerene wire within the channel of the COF. The 0.20 eV width of the C_{60} conduction band provides an energetic driving force for any electrons in the C_{60} conduction band to relax to the lower band. This means that excited electron density in the pocket-bound fullerene orbitals would initially delocalize across the adjacent pore fullerene, and subsequently localize onto the channel fullerenes. Combined with the initial driving force for charge transfer, this additional force would promote charge separation at the COF-C_{60} interface as well as transfer of the free electron into the 1-D fullerene wire in the nearby channel.

Molecular dynamics simulations

The structural stability of **NEUCOF1**-C_{60} dispersion-bound complexes at OPV operating conditions is crucial to the ability of these co-crystals to act as OPV materials. The PW-DFT calculations described above were performed on idealized 0 K structures, but OPVs operate at elevated temperatures. To determine this stability, we have employed molecular dynamics simulations on three **NEUCOF1**-C_{60} model systems. In the first of these simulations, fullerene molecules were placed into each of the binding pockets of the **NEUCOF1** 1-D wire analogue described in the Computational Methods section, and a 2 ns NVT simulation was propagated at 350 K, above typical OPV operating temperatures. At this temperature the C_{60} molecules remain within their binding pockets (Figure 7), which suggests that the dispersion intermolecular forces are held between the fullerenes and the framework. The second simulation was performed on the 3-D periodic model of **C**, with fullerene molecules in all of the binding pockets as well as the channel sites. The NVT simulation of this co-crystal at 350 K shows similar results to those of the wire simulation. The C_{60} molecules housed in the binding pockets remain in those pockets throughout the simulation. Additionally, the channel fullerenes associate with the pocket-bound molecules and form a fullerene network throughout the COF. Of particular note in this simulation is the short distance between all four of the fullerene molecules in the cell; the largest of these distances is 3.5 Å while non-covalent π-π interactions have been observed at distances up to 5.0 Å.[52] Therefore, all of the fullerene molecules in the simulation are near enough to participate in a conductive fullerene network.

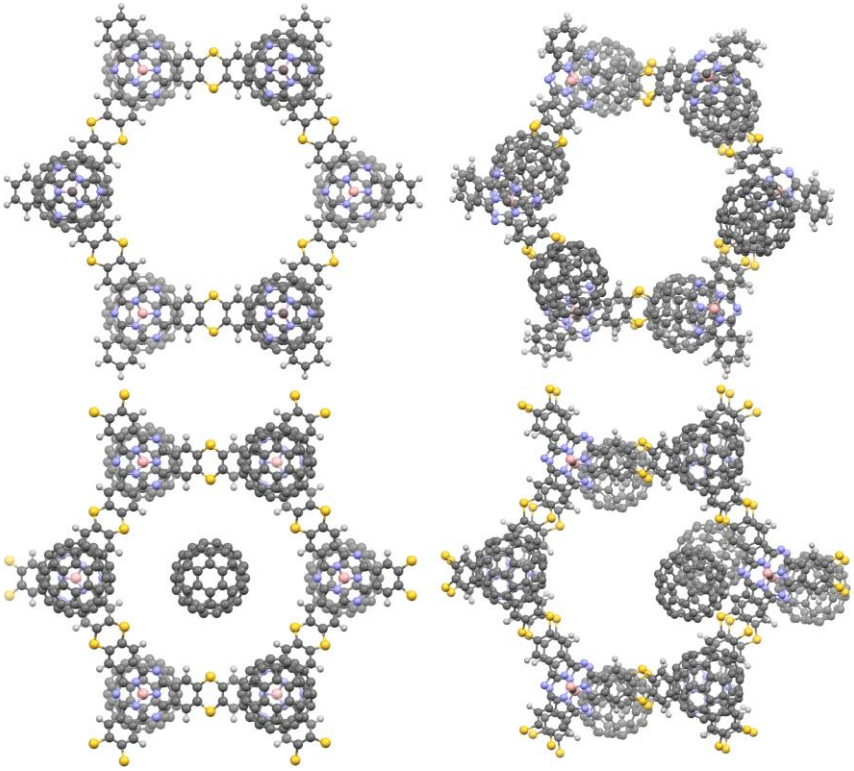

Figure 7. Snapshots of (left) initial and (right) final configurations of **NEUCOF1** MD simulations at 350 K viewed along the pore direction, [001]. (Top) 1D wire analogue of **NEUCOF1** with filled binding pockets, (bottom) co-crystal **C**.

We performed a third MD simulation on the **NEUCOF1** 1-D wire analogue to determine the ability of **NEUCOF1** to adsorb fullerene guests into its binding pockets. The model for this simulations includes twelve fullerene molecules with six available binding pockets per cell to ensure that some fullerenes would be left over after all of the binding pockets were filled. The **NEUCOF1** 1-D wire empty and fullerenes are distributed in the surrounding void space as shown in Figure 8.

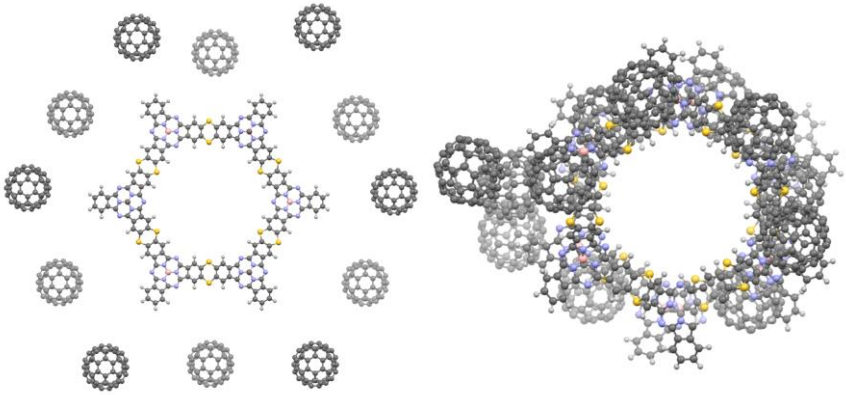

Figure 8. Snapshots of (left) initial and (right) final configurations of 1-D wire analogue of **NEUCOF1** in a fullerene-filled environment, viewed along pore direction, [001].

Another 2 ns NVT simulation shows that these fullerenes migrate from their initial positions into the binding pockets of **NEUCOF1**. The thianthrene linkage promotes structural flexibility to reorganize as the fullerenes are accommodated. This simulation shows that these additional fullerene molecules will bind fullerenes in empty peripheral pockets via π–π interactions.

Disorder effects on electronic structure

While MD simulations show that the COF-C_{60} co-crystals are predicted to be stable from 0–350 K, they also show a significant increase in structural disorder. We computed the band structure to determine the effect of thermal fluctuations on the electronic structure relative to the 0 K structures. Figure 9 shows the computed band structure of **C** post-MD simulation. The fullerene conduction band group in this disordered structure has a width of 0.36 eV, the same as for **C** at 0 K. Some of the individual bands appear to flatten out at higher temperature, which suggests that the orbitals are more localized onto individual molecules than in the 0 K structure, while the 0.36 eV width suggests that the fullerenes are still interacting. Therefore, thermal effects have a minor effect on the band structure and the co-crystal maintains its desirable electronic structure at typical operating temperatures.

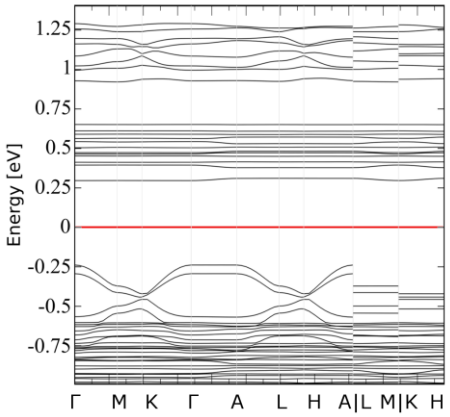

Figure 9. Band structure plot for final configuration of MD simulation of co-crystal **C**. Energy is plotted relative to the Fermi level, shown by red line, and vertical dashed lines show high-symmetry points.

Conclusions

We have designed a new SubPc-based COF (**NEUCOF1**) to function as an electron-donating scaffold for next-generation co-crystalline OPV devices. **NEUCOF1** can dock fullerene C_{60} acceptors and binds them in a ball-and-socket motif via its 17.4 Å binding pockets and the adjacent 17.9 Å unidirectional channels, likely to form COF-C_{60} co-crystals. We used PW-DFT methods to minimize the geometries of **NEUCOF1** and three COF-C_{60} co-crystals. The structural stability of the COF-C_{60} co-crystals was assessed using MD simulations, which show that fullerenes in the binding pockets remain dispersion-bound up to at least 350 K and maintain favorable interaction distances within the C_{60} nanowire. Our computed band structures at 0K and 350 K are consistent with sunlight absorption followed by a series of downhill charge transfer and charge separation processes resulting in photocurrent. Our calculations show a driving force of 0.27 eV for exciton charge transfer to the pocket-bound fullerenes. Charge separation could then occur at the COF-C_{60} D-A interface, followed by the transfer of the free electron to the nanowire of C_{60} acceptors with a driving force of 0.20 eV. The high internal surface area of the COF combined with directional

charge transport via columns of acceptor molecules, could overcome the competition between D-A surface area and long-range order in current OPV architectures. Due to the promising structural and electronic properties of this material, further theoretical characterization of a family of related COFs is underway, and experimental synthesis and characterization are forthcoming.

Acknowledgements. The authors acknowledge the Department of Chemistry & Chemical Biology for financial support. The high-performance computing resourced provided by the Massachusetts Green High-Performance Computing Center (MGHPCC), and the Northeastern High Performance (Discovery cluster).

Author Contributions. S. A. Lopez conceived of the project and supervised the co-authors obtaining the results and the analysis thereof. J. M. Cox wrote the majority of the manuscript, performed many of the quantum mechanical calculations of the optimized structures, and band structures. J. M. Cox assisted B. Mileson in the set-up and oversaw the analysis of the remaining quantum mechanical calculations of the optimized structures, band structures, and DOSs. J. M. Cox assisted A. Sadagopan in the set-up and oversaw the analysis of the molecular dynamics simulations. All authors contributed to the manuscript.

Competing Interests statement. The authors declare no conflicts of interest.

Supporting Information. The Supporting Information is available free of charge and includes a visualization of high-symmetry k-path used for band structures, RMSD plots for MD simulations, orbital images, unit cells and fractional coordinates for PW-DFT models.

References

1. Hedley, G. J.; Ruseckas, A.; Samuel, I. D. W., Light Harvesting for Organic Photovoltaics. *Chemical Reviews* **2017,** *117* (2), 796-837.
2. Cheng, P.; Li, G.; Zhan, X.; Yang, Y., Next-Generation Organic Photovoltaics Based on Non-Fullerene Acceptors. *Nature Photonics* **2018,** *12* (3), 131-142.
3. Zhang, H.; Yao, H.; Hou, J.; Zhu, J.; Zhang, J.; Li, W.; Yu, R.; Gao, B.; Zhang, S.; Hou, J., Over 14% Efficiency in Organic Solar Cells Enabled by Chlorinated Nonfullerene Small-Molecule Acceptors. *Advanced Materials* **2018,** *30* (28), 1800613.
4. Meng, L.; Zhang, Y.; Wan, X.; Li, C.; Zhang, X.; Wang, Y.; Ke, X.; Xiao, Z.; Ding, L.; Xia, R., *et al.*, Organic and Solution-Processed Tandem Solar Cells with 17.3% Efficiency. *Science* **2018,** *361* (6407), 1094.
5. Mandoc, M. M.; Kooistra, F. B.; Hummelen, J. C.; de Boer, B.; Blom, P. W. M., Effect of Traps on the Performance of Bulk Heterojunction Organic Solar Cells. *Applied Physics Letters* **2007,** *91* (26), 263505.
6. Côté, A. P.; Benin, A. I.; Ockwig, N. W.; Keeffe, M.; Matzger, A. J.; Yaghi, O. M., Porous, Crystalline, Covalent Organic Frameworks. *Science* **2005,** *310* (5751), 1166.
7. Ning, G.-H.; Chen, Z.; Gao, Q.; Tang, W.; Chen, Z.; Liu, C.; Tian, B.; Li, X.; Loh, K. P., Salicylideneanilines-Based Covalent Organic Frameworks as Chemoselective Molecular Sieves. *Journal of the American Chemical Society* **2017,** *139* (26), 8897-8904.
8. Qian, H.-L.; Yang, C.-X.; Yan, X.-P., Bottom-up Synthesis of Chiral Covalent Organic Frameworks and Their Bound Capillaries for Chiral Separation. *Nature Communications* **2016,** *7*, 12104.

9. Yang, S.; Hu, W.; Zhang, X.; He, P.; Pattengale, B.; Liu, C.; Cendejas, M.; Hermans, I.; Zhang, X.; Zhang, J., *et al.*, 2d Covalent Organic Frameworks as Intrinsic Photocatalysts for Visible Light-Driven Co2 Reduction. *Journal of the American Chemical Society* **2018,** *140* (44), 14614-14618.
10. Wang, X.; Chen, L.; Chong, S. Y.; Little, M. A.; Wu, Y.; Zhu, W.-H.; Clowes, R.; Yan, Y.; Zwijnenburg, M. A.; Sprick, R. S., *et al.*, Sulfone-Containing Covalent Organic Frameworks for Photocatalytic Hydrogen Evolution from Water. *Nature Chemistry* **2018,** *10* (12), 1180-1189.
11. Kundu, T.; Wang, J.; Cheng, Y.; Du, Y.; Qian, Y.; Liu, G.; Zhao, D., Hydrazone-Based Covalent Organic Frameworks for Lewis Acid Catalysis. *Dalton Transactions* **2018,** *47* (39), 13824-13829.
12. Sun, B.; Zhu, C.-H.; Liu, Y.; Wang, C.; Wan, L.-J.; Wang, D., Oriented Covalent Organic Framework Film on Graphene for Robust Ambipolar Vertical Organic Field-Effect Transistor. *Chemistry of Materials* **2017,** *29* (10), 4367-4374.
13. Wu, C.; Liu, Y.; Liu, H.; Duan, C.; Pan, Q.; Zhu, J.; Hu, F.; Ma, X.; Jiu, T.; Li, Z., *et al.*, Highly Conjugated Three-Dimensional Covalent Organic Frameworks Based on Spirobifluorene for Perovskite Solar Cell Enhancement. *Journal of the American Chemical Society* **2018,** *140* (31), 10016-10024.
14. Li, B.-Q.; Zhang, S.-Y.; Wang, B.; Xia, Z.-J.; Tang, C.; Zhang, Q., A Porphyrin Covalent Organic Framework Cathode for Flexible Zn–Air Batteries. *Energy & Environmental Science* **2018,** *11* (7), 1723-1729.
15. Chen, L.; Furukawa, K.; Gao, J.; Nagai, A.; Nakamura, T.; Dong, Y.; Jiang, D., Photoelectric Covalent Organic Frameworks: Converting Open Lattices into Ordered Donor–Acceptor Heterojunctions. *Journal of the American Chemical Society* **2014,** *136* (28), 9806-9809.
16. Calik, M.; Auras, F.; Salonen, L. M.; Bader, K.; Grill, I.; Handloser, M.; Medina, D. D.; Dogru, M.; Löbermann, F.; Trauner, D., *et al.*, Extraction of Photogenerated Electrons and Holes from a Covalent Organic Framework Integrated Heterojunction. *Journal of the American Chemical Society* **2014,** *136* (51), 17802-17807.
17. Thomas, S.; Li, H.; Zhong, C.; Matsumoto, M.; Dichtel, W. R.; Bredas, J.-L., Electronic Structure of Two-Dimensional Π-Conjugated Covalent Organic Frameworks. *Chemistry of Materials* **2019**.
18. Hashemzadeh, H.; Raissi, H., Covalent Organic Framework as Smart and High Efficient Carrier for Anticancer Drug Delivery: A Dft Calculations and Molecular Dynamics Simulation Study. *Journal of Physics D: Applied Physics* **2018,** *51* (34), 345401.
19. Zhu, P.; Meunier, V., Electronic Properties of Two-Dimensional Covalent Organic Frameworks. *The Journal of Chemical Physics* **2012,** *137* (24), 244703.
20. Gutzler, R.; Perepichka, D. F., Π-Electron Conjugation in Two Dimensions. *Journal of the American Chemical Society* **2013,** *135* (44), 16585-16594.
21. Gutzler, R., Band-Structure Engineering in Conjugated 2d Polymers. *Physical Chemistry Chemical Physics* **2016,** *18* (42), 29092-29100.
22. Dogru, M.; Handloser, M.; Auras, F.; Kunz, T.; Medina, D.; Hartschuh, A.; Knochel, P.; Bein, T., A Photoconductive Thienothiophene-Based Covalent Organic Framework Showing Charge Transfer Towards Included Fullerene. *Angewandte Chemie International Edition* **2013,** *52* (10), 2920-2924.
23. Guo, J.; Xu, Y.; Jin, S.; Chen, L.; Kaji, T.; Honsho, Y.; Addicoat, M. A.; Kim, J.; Saeki, A.; Ihee, H., *et al.*, Conjugated Organic Framework with Three-Dimensionally Ordered Stable Structure and Delocalized Π Clouds. *Nature Communications* **2013,** *4*, 2736.

24. Kang, S. J.; Ahn, S.; Kim, J. B.; Schenck, C.; Hiszpanski, A. M.; Oh, S.; Schiros, T.; Loo, Y.-L.; Nuckolls, C., Using Self-Organization to Control Morphology in Molecular Photovoltaics. *Journal of the American Chemical Society* **2013,** *135* (6), 2207-2212.
25. Rhoda, H. M.; Kayser, M. P.; Wang, Y.; Nazarenko, A. Y.; Belosludov, R. V.; Kiprof, P.; Blank, D. A.; Nemykin, V. N., Tuning up an Electronic Structure of the Subphthalocyanine Derivatives toward Electron-Transfer Process in Noncovalent Complexes with C60 and C70 Fullerenes: Experimental and Theoretical Studies. *Inorganic Chemistry* **2016,** *55* (19), 9549-9563.
26. Gotfredsen, H.; Holmstrøm, T.; Muñoz, A. V.; Storm, F. E.; Tortzen, C. G.; Kadziola, A.; Mikkelsen, K. V.; Hammerich, O.; Nielsen, M. B., Complexation of Fullerenes by Subphthalocyanine Dimers. *Organic Letters* **2018,** *20* (18), 5821-5825.
27. Konarev, D. V.; Troyanov, S. I.; Lyubovskaya, R. N., Coordination Complex of Boron Subphthalocyanine (Bsubpc) with Fluorenone Pinacolate: Effective Π–Π Interaction of Concave Bsubpc Macrocycle with Fullerene C60. *CrystEngComm* **2015,** *17* (21), 3923-3926.
28. Claessens, C. G.; González-Rodríguez, D.; Rodríguez-Morgade, M. S.; Medina, A.; Torres, T., Subphthalocyanines, Subporphyrazines, and Subporphyrins: Singular Nonplanar Aromatic Systems. *Chemical Reviews* **2014,** *114* (4), 2192-2277.
29. Mutolo, K. L.; Mayo, E. I.; Rand, B. P.; Forrest, S. R.; Thompson, M. E., Enhanced Open-Circuit Voltage in Subphthalocyanine/C60 Organic Photovoltaic Cells. *Journal of the American Chemical Society* **2006,** *128* (25), 8108-8109.
30. Garner, R. K.; Josey, D. S.; Nyikos, S. R.; Dovijarski, A.; Wang, J. M.; Evans, G. J.; Bender, T. P., Boron Subphthalocyanines as Electron Donors in Outdoor Lifetime Monitored Organic Photovoltaic Cells. *Solar Energy Materials and Solar Cells* **2018,** *176*, 331-335.
31. Pandey, R.; Gunawan, A. A.; Mkhoyan, K. A.; Holmes, R. J., Efficient Organic Photovoltaic Cells Based on Nanocrystalline Mixtures of Boron Subphthalocyanine Chloride and C60. *Advanced Functional Materials* **2012,** *22* (3), 617-624.
32. Sánchez-Molina, I.; Claessens, C. G.; Grimm, B.; Guldi, D. M.; Torres, T., Trapping Fullerenes with Jellyfish-Like Subphthalocyanines. *Chemical Science* **2013,** *4* (3), 1338-1344.
33. Sánchez-Molina, I.; Grimm, B.; Krick Calderon, R. M.; Claessens, C. G.; Guldi, D. M.; Torres, T., Self-Assembly, Host–Guest Chemistry, and Photophysical Properties of Subphthalocyanine-Based Metallosupramolecular Capsules. *Journal of the American Chemical Society* **2013,** *135* (28), 10503-10511.
34. Cabaleiro-Lago, E. M.; Rodríguez-Otero, J.; Carrazana-García, J. A., A Theoretical Study of Complexes between Fullerenes and Concave Receptors with Interest in Photovoltaics. *Physical Chemistry Chemical Physics* **2017,** *19* (39), 26787-26798.
35. Sato, K.; Pradhan, E.; Asahi, R.; Akimov, A. V., Charge Transfer Dynamics at the Boron Subphthalocyanine Chloride/C60 Interface: Non-Adiabatic Dynamics Study with Libra-X. *Physical Chemistry Chemical Physics* **2018,** *20* (39), 25275-25294.
36. Ong, W. J.; Swager, T. M., Dynamic Self-Correcting Nucleophilic Aromatic Substitution. *Nature Chemistry* **2018,** *10* (10), 1023-1030.
37. Kresse, G.; Hafner, J., Ab Initio Molecular Dynamics for Liquid Metals. *Physical Review B* **1993,** *47* (1), 558-561.
38. Kresse, G.; Hafner, J., Ab Initio Molecular-Dynamics Simulation of the Liquid-Metal--Amorphous-Semiconductor Transition in Germanium. *Physical Review B* **1994,** *49* (20), 14251-14269.

39. Kresse, G.; Furthmüller, J., Efficiency of Ab-Initio Total Energy Calculations for Metals and Semiconductors Using a Plane-Wave Basis Set. *Computational Materials Science* **1996,** *6* (1), 15-50.
40. Kresse, G.; Furthmüller, J., Efficient Iterative Schemes for Ab Initio Total-Energy Calculations Using a Plane-Wave Basis Set. *Physical Review B* **1996,** *54* (16), 11169-11186.
41. Grimme, S.; Ehrlich, S.; Goerigk, L., Effect of the Damping Function in Dispersion Corrected Density Functional Theory. *Journal of Computational Chemistry* **2011,** *32* (7), 1456-1465.
42. Mori-Sánchez, P.; Cohen, A. J.; Yang, W., Localization and Delocalization Errors in Density Functional Theory and Implications for Band-Gap Prediction. *Physical Review Letters* **2008,** *100* (14), 146401.
43. Setyawan, W.; Curtarolo, S., High-Throughput Electronic Band Structure Calculations: Challenges and Tools. *Computational Materials Science* **2010,** *49* (2), 299-312.
44. Momma, K.; Izumi, F., Vesta 3 for Three-Dimensional Visualization of Crystal, Volumetric and Morphology Data. *Journal of Applied Crystallography* **2011,** *44* (6), 1272-1276.
45. Stephens, P. J.; Devlin, F. J.; Chabalowski, C. F.; Frisch, M. J., Ab Initio Calculation of Vibrational Absorption and Circular Dichroism Spectra Using Density Functional Force Fields. *The Journal of Physical Chemistry* **1994,** *98* (45), 11623-11627.
46. Dunning, T. H., Gaussian Basis Sets for Use in Correlated Molecular Calculations. I. The Atoms Boron through Neon and Hydrogen. *The Journal of Chemical Physics* **1989,** *90* (2), 1007-1023.
47. Woon, D. E.; Dunning, T. H., Gaussian Basis Sets for Use in Correlated Molecular Calculations. Iii. The Atoms Aluminum through Argon. *The Journal of Chemical Physics* **1993,** *98* (2), 1358-1371.
48. Kendall, R. A.; Dunning, T. H.; Harrison, R. J., Electron Affinities of the First-Row Atoms Revisited. Systematic Basis Sets and Wave Functions. *The Journal of Chemical Physics* **1992,** *96* (9), 6796-6806.
49. Plimpton, S., Fast Parallel Algorithms for Short-Range Molecular Dynamics. *Journal of Computational Physics* **1995,** *117* (1), 1-19.
50. Harder, E.; Damm, W.; Maple, J.; Wu, C.; Reboul, M.; Xiang, J. Y.; Wang, L.; Lupyan, D.; Dahlgren, M. K.; Knight, J. L., *et al.*, Opls3: A Force Field Providing Broad Coverage of Drug-Like Small Molecules and Proteins. *Journal of Chemical Theory and Computation* **2016,** *12* (1), 281-296.
51. Borlido, P.; Aull, T.; Huran, A. W.; Tran, F.; Marques, M. A. L.; Botti, S., Large-Scale Benchmark of Exchange–Correlation Functionals for the Determination of Electronic Band Gaps of Solids. *Journal of Chemical Theory and Computation* **2019,** *15* (9), 5069-5079.
52. Headen, T. F.; Howard, C. A.; Skipper, N. T.; Wilkinson, M. A.; Bowron, D. T.; Soper, A. K., Structure of Π−Π Interactions in Aromatic Liquids. *Journal of the American Chemical Society* **2010,** *132* (16), 5735-5742.

TOC Graphic

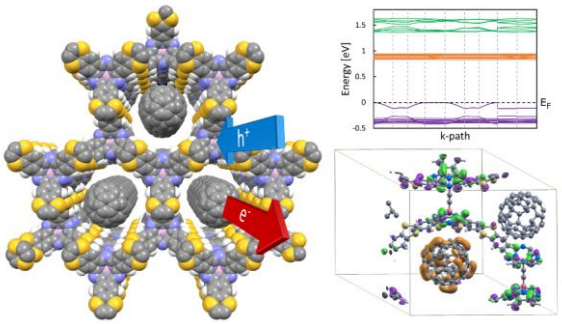
h+
e-
1.5
1
0.5
0
-0.5
Energy [eV]
E_F
k-path